Contemporary Engineering Sciences, Vol. 13, 2020, no. 1, 335 - 349
HIKARI Ltd, www.m-hikari.com
https://doi.org/10.12988/ces.2020.91605

Fatigue Behavior of a Riveted Connection Detail Used in Steel Bridge Construction

Warda Abdulla

Auburn Science and Engineering Center (ASEC 210)
Department of Civil Engineering, The University of Akron
Akron, OH, 44325-3905, USA

Craig Menzemer

Auburn Science and Engineering Center (ASEC 210)
Department of Civil Engineering, The University of Akron,
Akron, OH, 44325-3905, USA

Abstract

Riveted steel grating is often used in movable bridges and may be considered as a lightweight alternative for structures limited by dead loads. Bridges are subjected to repeated loading and are susceptible to localized fatigue cracking. This particular study focused on the fatigue behavior of the riveted connection found in some heavy steel gratings, as both open-hole and riveted coupon fatigue test results are compared to tests of heavy-duty steel grating. Fracture surface features associated with the test specimens are discussed. Finite element modeling of the riveting process illustrates development of favorable residual stresses, consistent with fatigue test results.

Keywords: riveted connection; S-N curve; riveted sample modeling; residual stresses; fracture surfaces

1. Introduction

Heavy duty riveted steel grating has been utilized as bridge deck for well over

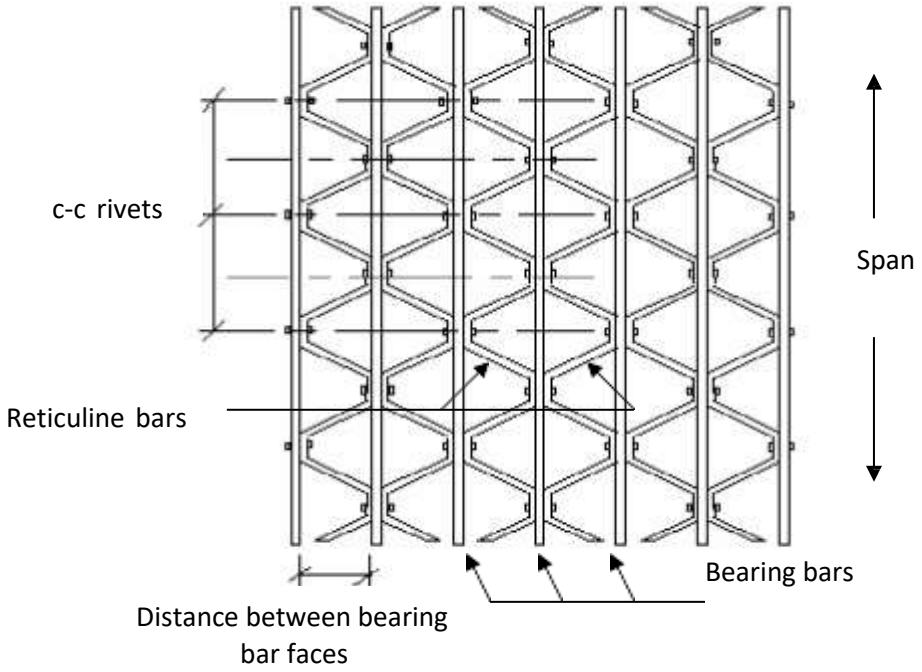

Figure 1: Riveted Grating [1]

70 years. Figure 1 illustrates the different components of a standard riveted steel grate. Lightweight versions of the deck are often produced by replacing every other bearing bar with smaller intermediate bars. Bearing bars may be oriented either parallel or transverse to the direction of traffic [1], [2]. Figure 2 shows a riveted deck that has been in service on a movable bridge for more than 40 years [3].

A large number of research studies have focused on the static and fatigue behavior of heavy-duty welded deck systems. GangaRao tested and evaluated a number of steel deck samples under both static and fatigue loads. Details found on a number of welded deck systems were found to be consistent with a Category E fatigue resistance. A smaller number of riveted samples were found to have improved performance as compared to available welded decks [4]. Fetzer tested eight different types of steel grating, including both welded and riveted. Stiffness parameters were evaluated and used as input to finite element models.

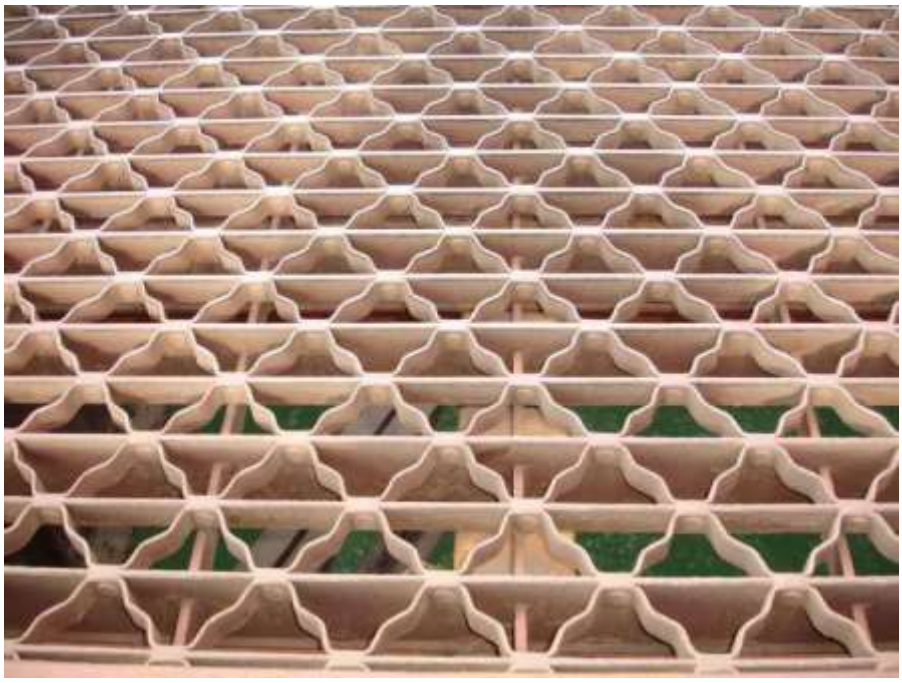

Figure 2: Riveted Steel Deck in Service [3]

Fatigue tests demonstrated that puddle welds on certain welded deck systems to be categorized as E' [5]. Other alternative welds had a variety of categorized fatigue strengths.

2. Fatigue Testing – Coupon Specimens

A1011 steel coupon samples were machined from blanks removed from rectangular steel bearing bar strip. Specimen types included both open-hole and riveted. Rivets were taken from stock currently utilized in the manufacture of riveted steel grate systems. Rivets were C1010 steel. Figure 3 depicts the types of samples used in this study.

Specimens measured 36.7 cm (14.5 in) in length and were ¼ in thick. Test sections were 12.7 cm (5 in) in length and measured 2.54 cm (1in) in width. Holes in the specimens were punched and measured a nominal 0.953cm (0.375 in). A total of 20 open hole specimens and 18 riveted specimens were tested at stress ranges that varied from 124.1 to 241.3 MPa (18 to 35 ksi). Tension – tension fatigue loads at an R ratio of 0.1 were used to test the specimens. Loads were applied at 10 Hz until failure. Run-outs were considered to have occurred if 10,000,000 load cycles were applied without failure.

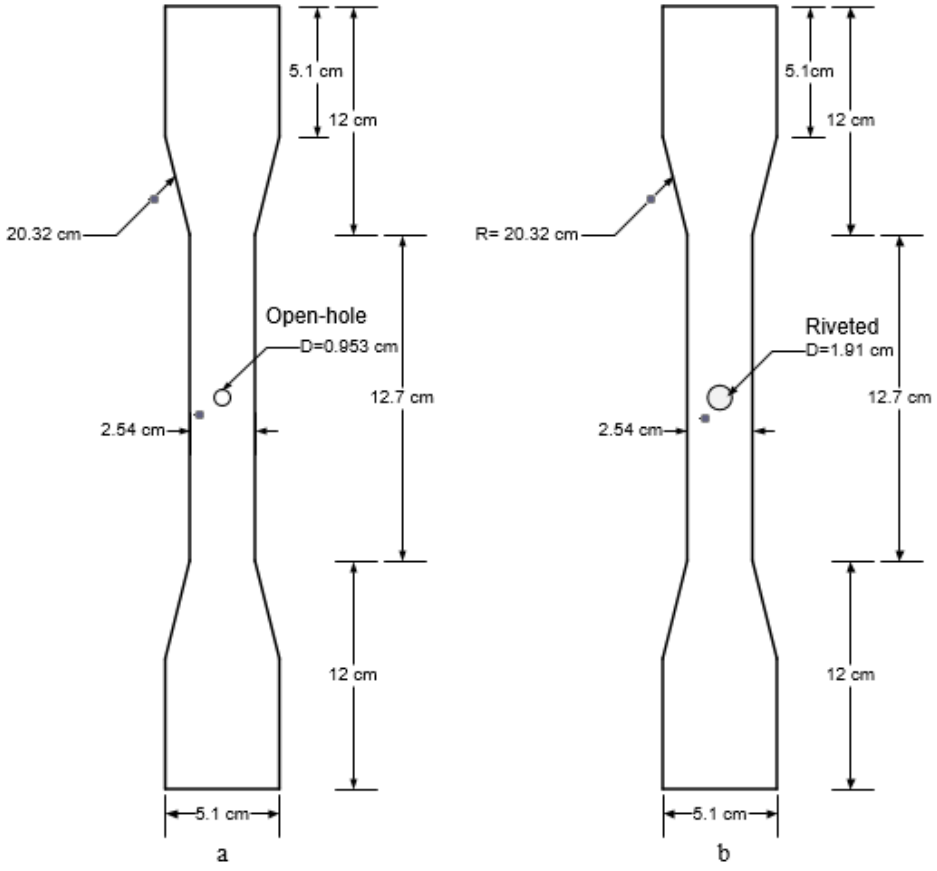

Figure 3: Geometry of Open hole (a) and Riveted Coupon Samples (b)

Figure 4 shows the test results for both the open hole and riveted coupon specimens along with their best fit lines. What is interesting to note is that the primary difference in the open hole and riveted coupons is the addition of the rivet. Addition of the rivet has increased fatigue life for all, but the highest stress ranges used in the study. Further, the best fit line for the riveted specimens has a shallower slope as compared to the best fit line for the open hole samples.

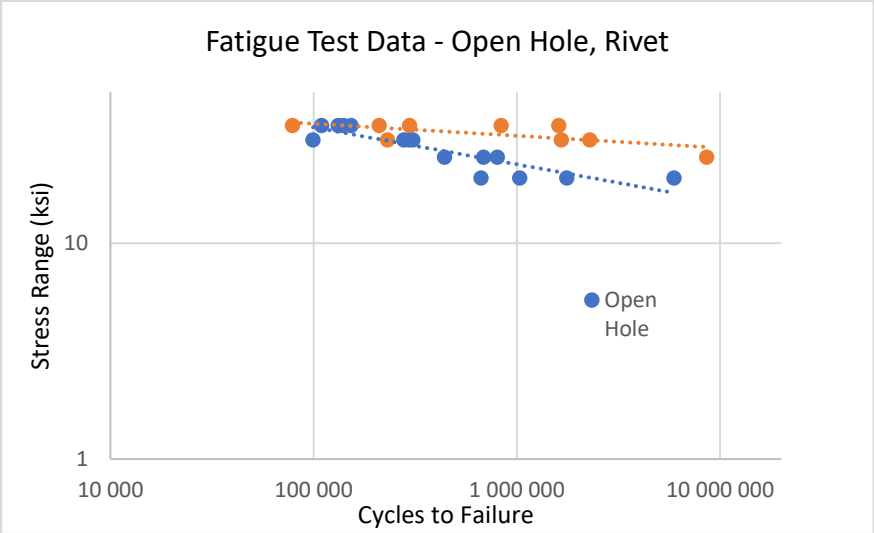

Figure 4: Fatigue Test Results for Open Hole and Riveted Coupons

Figure 5 shows the test data for both the open hole as well as the riveted coupons for which the life was greater than 1,000,000 cycles. It is important to note that a runout was taken as a specimen that did not fail after 10,000,000 cycles. Runouts occurred at a greater frequency and larger stress ranges for the riveted coupons as compared to the open hole specimens. Runouts occurred for riveted specimens above 172.4 MPa (25 ksi), while no runouts were observed for open hole specimens above 124.1MPa (18 ksi). Assuming the constant amplitude fatigue limit (CAFL) to occur around 10,000,000 cycles, the riveted coupon CAFL is at least 48.3 MPa (7 ksi) greater than the open hole specimens.

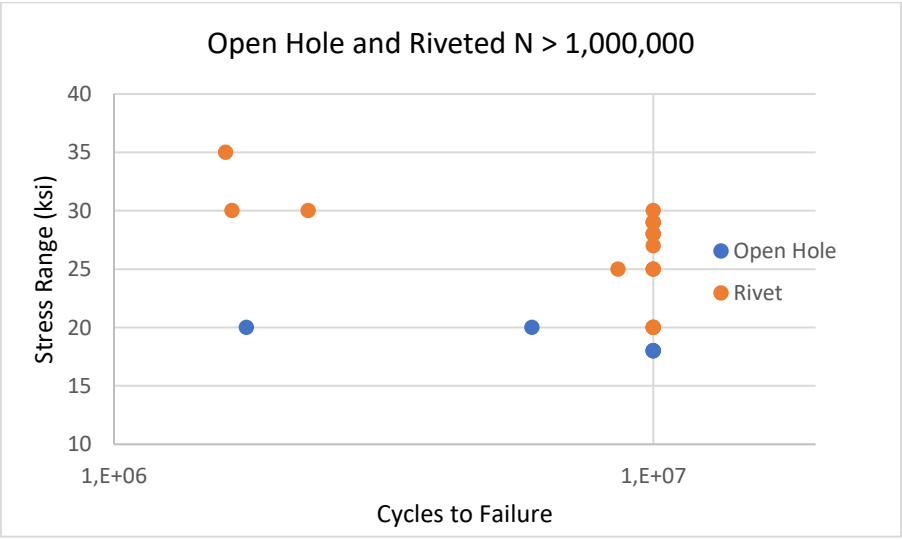

Figure 5: Open Hole and Riveted Coupons with N > 1,000,000 cycles

Figure 6 compares the fatigue test data and best fit lines for the open hole, riveted coupon and steel grate test samples. It is clear that the open hole test results are more consistent with the steel grate component tests and as compared to the riveted coupon specimens.

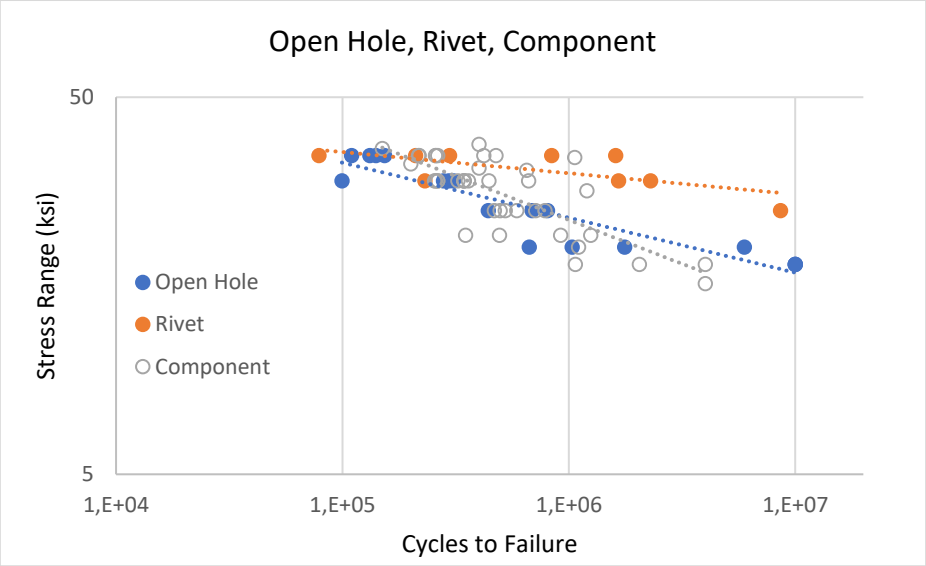

Figure 6: Fatigue Test Results: Open Hole, Riveted Coupon and Components

3. Finite Element Modeling – Rivet Driving

Riveting was conducted in three steps: 1) the rivet was inserted into the punched hole, 2) a load was used to squeeze the rivet and fill the hole and 3) the load was removed.

Solid C1010 steel rivets were used throughout this series of tests and are often utilized in the manufacture of steel grates. Figure 7 shows a C1010 rivet along with a typical stress – strain response curve evaluated from a sub-size tensile specimen removed from the shank of a rivet. The stress – strain response is consistent with that of a low carbon steel, with a yield point of 427.5 MPa (62 ksi) and an ultimate strength of nearly 482.6 MPa (70 ksi). An average stress – strain curve was utilized in the finite element model to assess the stresses resulting from rivet driving.

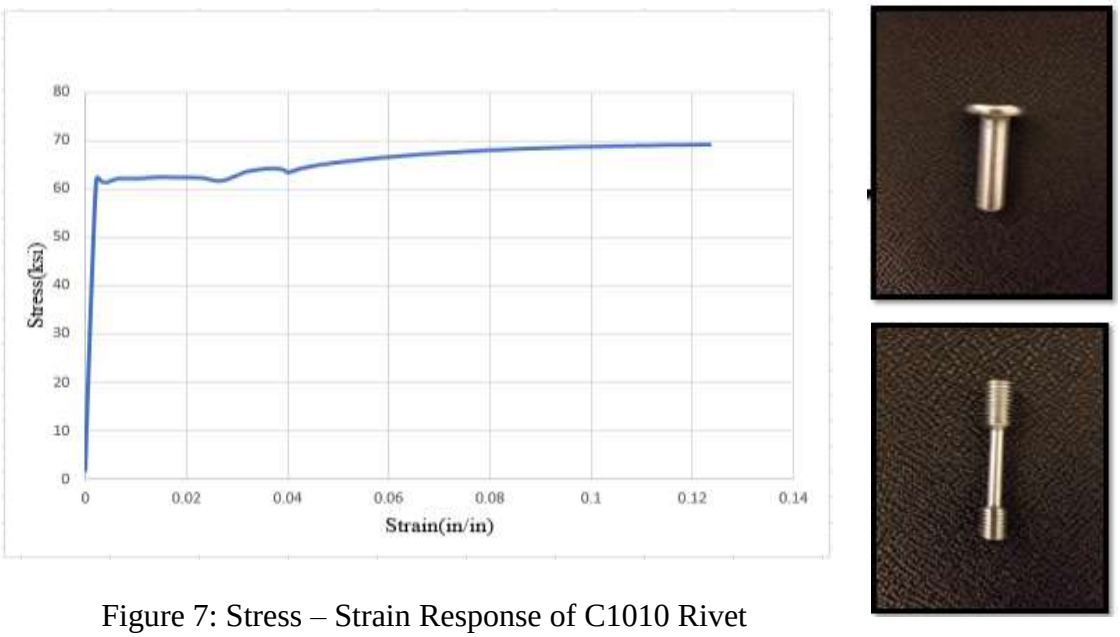

Figure 7: Stress – Strain Response of C1010 Rivet

A quarter model of an open hole, dogbone shaped specimen was constructed using three dimensional solid elements in Abaqus/ CAE 6.14-5. The rivet hole was created with a radius of 0.4763 cm (0.1875 in) using the create circle feature. A rivet model was constructed separately, consisting of a cylindrical body with a shank diameter of 0.953 cm (0.375in), inserted through the hole in the plate using the create constraint coaxial feature. The material for both the rivet and specimen is assumed to behave in an elastic perfectly plastic (MEPP) manner, with a Young's modulus of 199948 MPa (29000 ksi) and Poisson's ratio of 0.3 in the elastic range. Figure 8 shows the stress-strain curve taken from tensile tests of a bearing bar that was used to represent the material of the specimen. Additionally, the analysis was taken to be nonlinear. In order to allow the rivet and specimen to interact with each other, 3 surface to surface contacts were defined: (i) between the plate top face and rivet top face (ii) between the plate bottom face and rivet bottom face, and (iii) the hole interior and rivet shank [6].

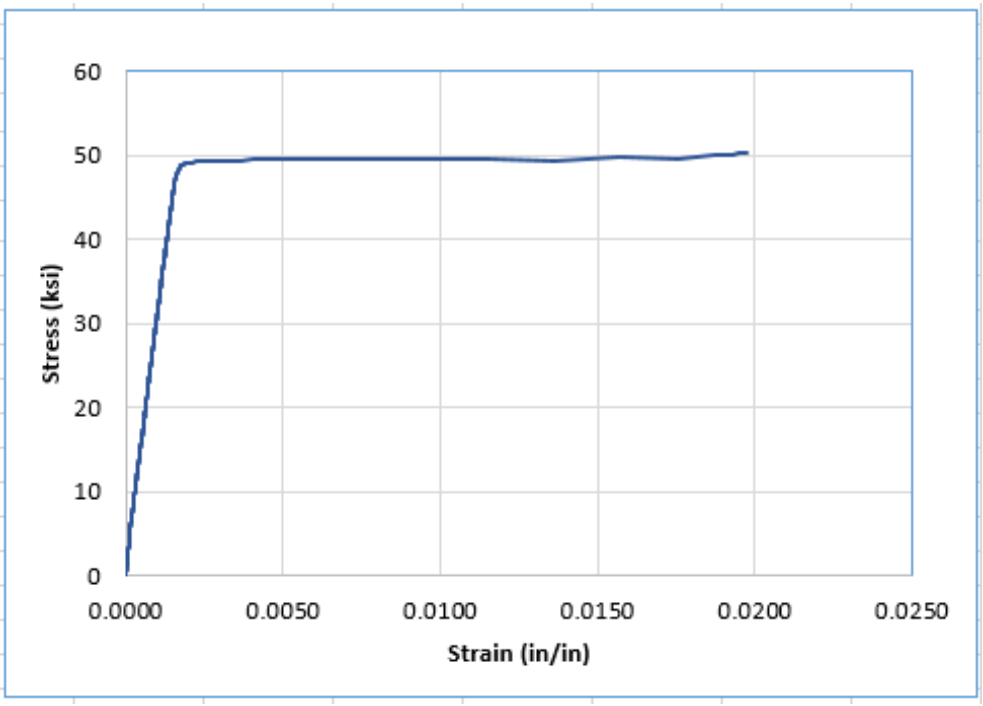

Figure 8: Stress – Strain Response of Bearing Bar Material

Figure 9 depicts the model along with the mesh. The finite element model utilized about 10,000 C3D20 elements from the ABAQUS library, with about 48,000 nodes and 284,000 degrees of freedom. The Finite-Element stress distribution for the plate and rivet installed with squeeze force (Fsq) of 95.15 MPa (13.8 kips) is shown in Figure 10 after the squeeze load is removed. The squeeze load was applied as a distributed force over the head of the rivet. Unloading the rivet results in residual stress, which, as expected, varies from tension to compression. Compression residual stresses exist inside the hole, varying from a maximum stress of nearly -303.4 MPa (-44 ksi), to a positive tensile stress of less than 69 MPa (10 ksi) away from the edge of the rivet (Figure 11). This is consistent with the fatigue behavior observed during the tests.

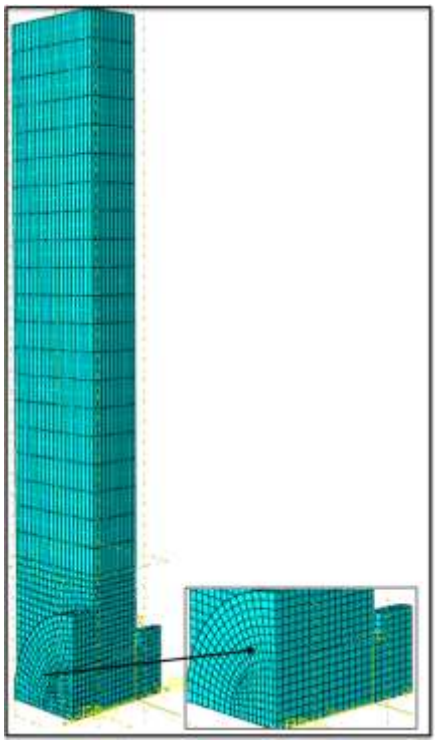

Figure 9: Mesh for Rivet Specimen Model [6]

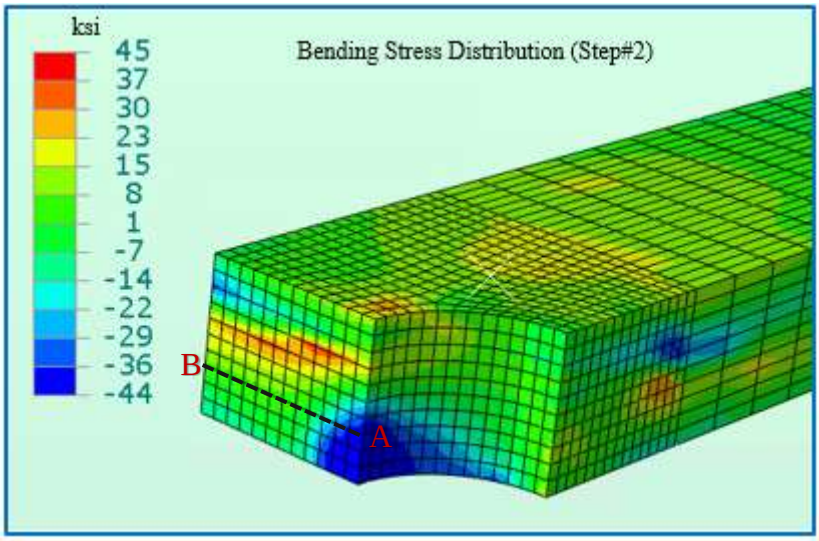

Figure 10: Resulting Longitudinal Stress Distribution after Squeeze Load Removed [6]

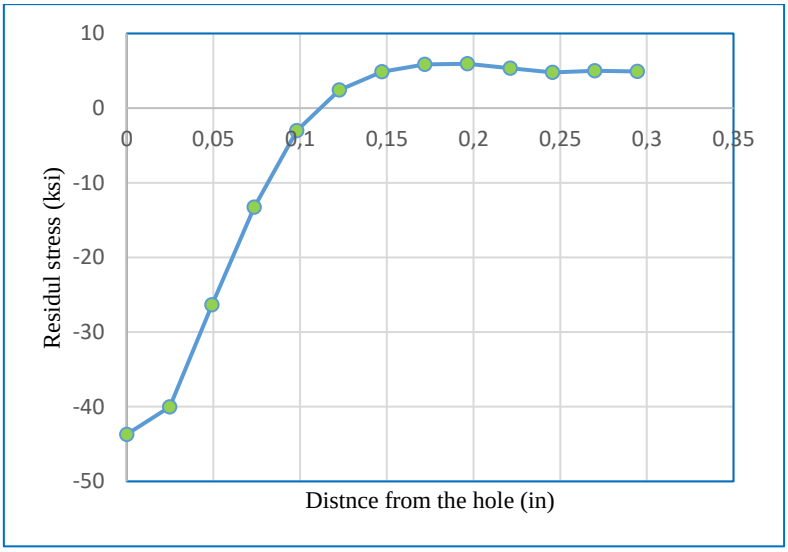

Figure 11: Residual Stress Along Cross Section A-B

4. Fracture Surface Examination

Fracture surfaces of several failed fatigue test samples were examined in a Scanning Electron Microscope (SEM). Sections were removed from two specimens, both open-hole and riveted coupons, tested at an identical stress range of 206.8 MPa (30ksi). Each sample was tested at a frequency of 10 Hz until failure. Four samples for each specimen were examined, one on either side of the hole, as well as the top and bottom surfaces as shown in Figure 12 and 13 respectively. Visual examination shows that the origin of the fatigue cracking was in the corner of the hole.

Figure 12: Top and bottom sections of the open-hole sample

Figure 13: Top and bottom sections of the riveted sample

SEM inspection was conducted at different magnification levels ranging between 33X to 10,000X. Observation in the SEM allows determination of the mechanisms associated with cracking. A comparison of the striation spacing between the two different sample types should allow an evaluation of differences in growth rate and indirectly provide a measure of the effect of the riveting process on fatigue behavior.

4-1 Open-hole Coupon Top Surface Adjacent to Hole

Figure 14(a) shows the overall morphology and visually reveals a rather smooth fracture surface texture. The topographic features present crack progression marks and indicate a change of the position of the fatigue crack front. Figure 14(b) presents an abundance of dimples and microvoids on the fracture surface. Microvoid coalescence is most often associated with overload and final separation. Equiaxed dimples are generally indicative of tensile loading and are consistent with the tests. Higher magnification of (b) shows microscopic voids of varying size with ductile dimples on the fracture surface (Figure 14(c)). A macroscopically smooth region reveals striations, which are associated with fatigue crack propagation. Pockets of shallow striations in the region are observed along with secondary cracks (Figure 14(d)).

4-2 Open-hole Coupon Bottom Surface Adjacent to the Hole

A region representative of stable crack growth is shown in figure 15 (a)). Higher magnification of an area clearly shows both ductile and brittle striations, which are representative of fatigue (Figure 15 (b)). Secondary cracking on the fracture surface is apparent.

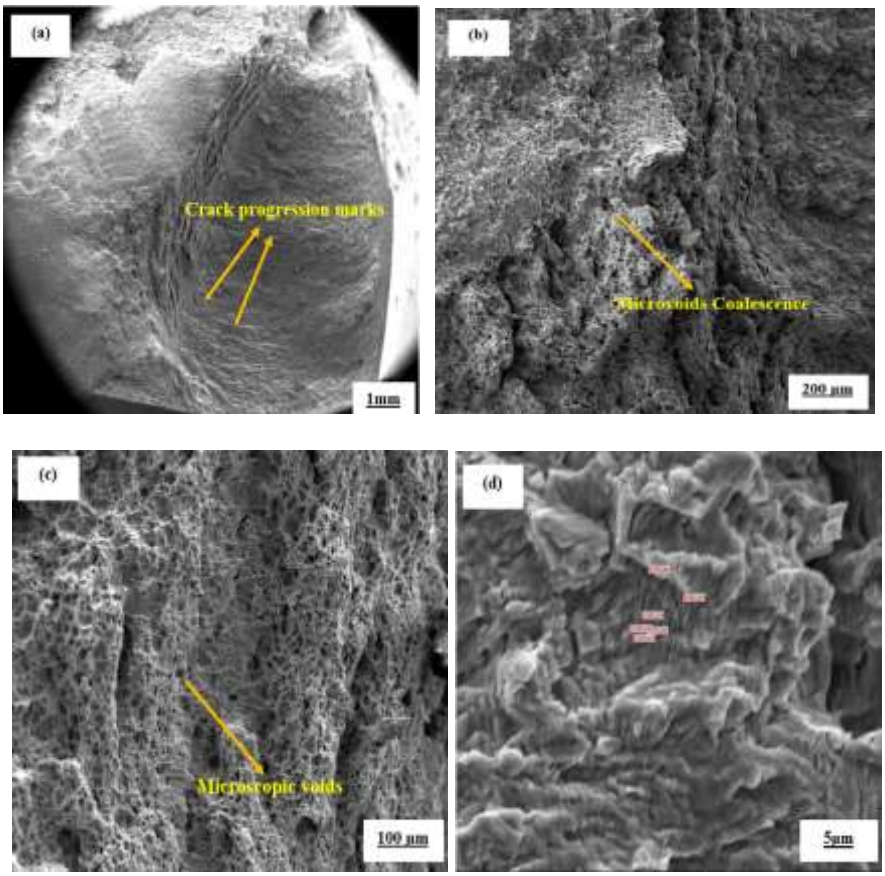

Figure 14: Scanning electron micrographs of the fatigue fracture surface of the open-hole showing (a) overall morphology of failure (b) microvoid coalescence (c) microscopic voids (d) pockets of shallow striations

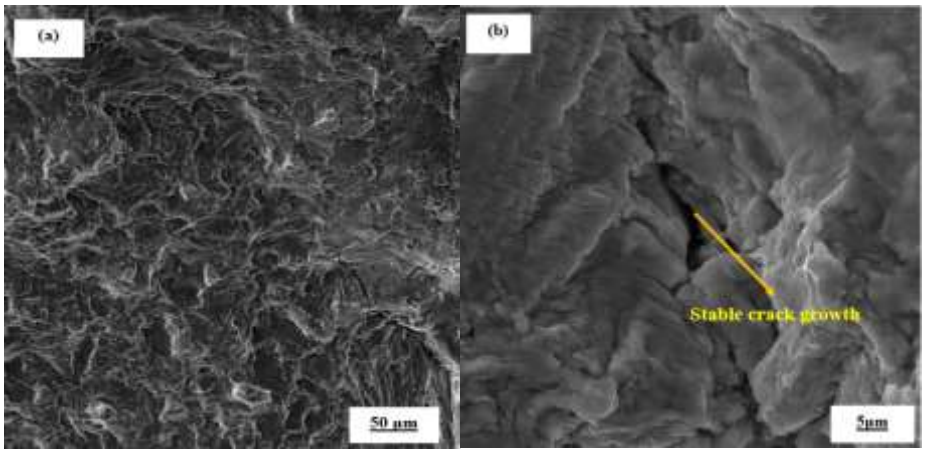

Figure 15: Scanning electron micrographs of the fatigue fracture surface of the open-hole showing (a) stable crack growth along the rough region (b) ductile and brittle striations

4-3 Riveted Coupon Top Surface Adjacent to the Hole

Overall morphology of the failure surface shows a region of distinct demarcation between fatigue and overload (Figure 16 (a)). Higher magnification observation of the smooth region revealed crack initiation (Figure 16 (b)). Figure 16 (c) shows shallow striations intermingled with fine microscopic cracks. High magnification observation of the region of early microscopic crack growth revealed pockets of distinct striations randomly spaced and oriented (Figure 16 (d))

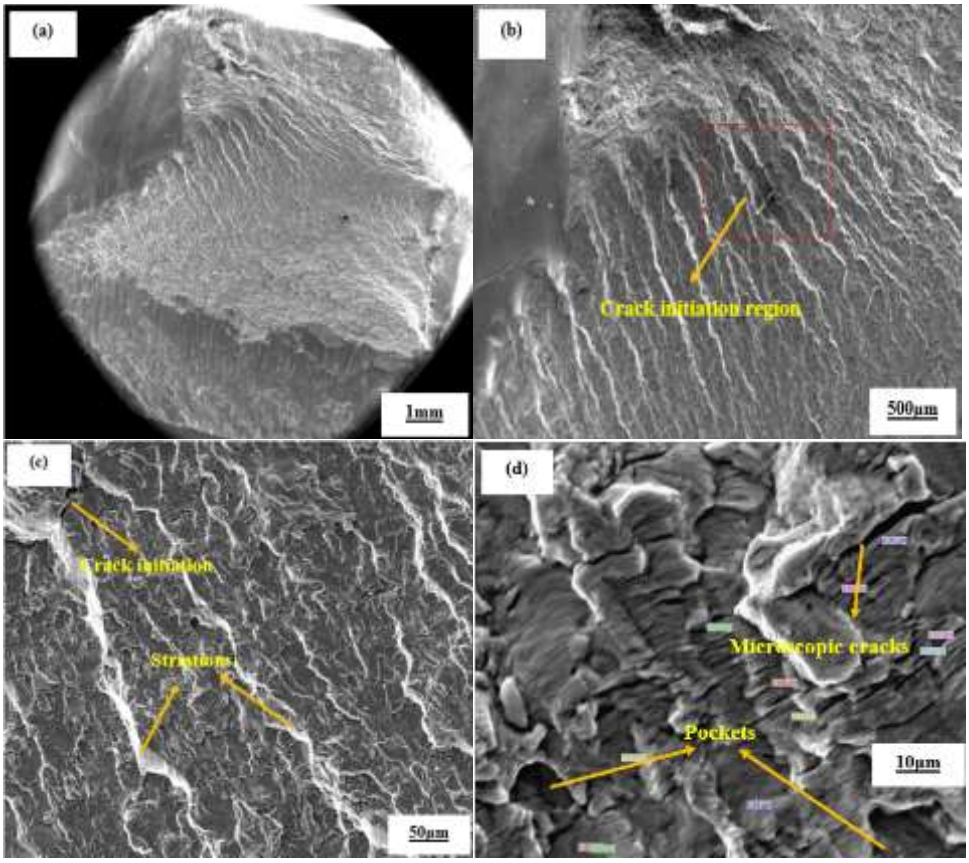

Figure 16: Scanning electron micrographs of the fatigue fracture surface of the riveted showing (a) overall morphology of failure (b) crack initiation area (c) shallow striations (d) microscopic cracks and pockets

4-4 Riveted Coupon Bottom Adjacent the Hole

Overall morphology of the failure is predominantly rough (Figure 17 (a)). Figure 17 (b) shows the overall fatigue propagation direction. Higher magnification observation of the fracture surface reveals a noticeable population of voids of varying size and microvoid coalescence with a rich array of ductile dimples (Figure 17 (c)). Figure 17 (d) presents striations intermingled with fine microscopic cracks.

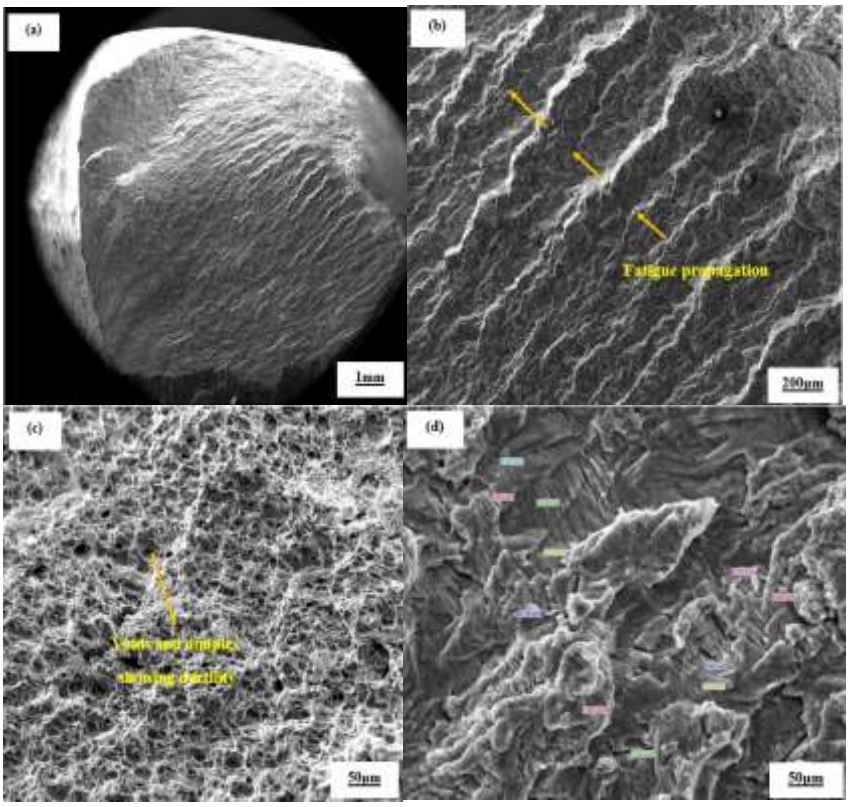

Figure 17: Scanning electron micrographs of the fatigue fracture surface of the riveted showing (a) overall morphology of failure (b) fatigue propagation direction (c) voids and dimples (d) striations along with early microscopic cracks

5. Conclusions

The main conclusions of this study are as follows:

1. Data was presented inform of mean S-N curves for the open-hole and riveted coupons. The riveted coupons exhibited superior fatigue performance, particularly at longer lives.
2. Fatigue test results for the open-hole coupons indicated that the majority of failures occurred under 6,000,000 cycles and stress ranges larger than 124.1MPa (18ksi).
3. However, results obtained from the riveted coupon testing demonstrated that the majority of failures occurred under 8,700,000 cycles and stress ranges larger than 200 MPa (29ksi). This clearly shows the benefit of the riveting process.
4. Runout data for the riveted samples provides endurance limits (CAFL) at least 48.3 MPa (7ksi) greater than the open-hole coupons at 10 million cycles.
5. The best-fit S-N curve based on failure data of smaller size samples with open holes is consistent and shows reasonable agreement with the results of the actual riveted deck tests.

6. The scatter of the grate test results may have been influenced by the rivet installation process.
7. A finite element model of the specimen revealed the nature of the stress distribution around the hole and the plate.
8. Hot spot stresses observed in the finite element model were consistent with the failure regions, which tends to be in a good agreement with the experimental results.
9. Within the limit of this study, SEM examination revealed that the fracture surfaces appeared to be characterized primarily by typical signs of microvoid coalescence-type with transgranular paths. Fatigue cracking was also evident with the existence of striations.

References

[1] ANSI / National Association of Architectural Metal Manufacturers (NAAMM), *Heavy Duty Metal Bar Grating Manual*, MBG 532-09 (2009), 5th Edition.
[2] Chavel, B., *Steel Bridge Design Handbook: Bridge Deck Design (FHWA-HIF-16-002)*, Vol. 17, 2015.
[3] Apperson, K. and Menzemer, C., *Heavy Duty Riveted Bridge Deck AASHTO H20 Loading and Fatigue Testing*, 13th Biennial Symposium of Heavy Movable Structures, Inc, 2010.
[4] Ganga Rao, H., Keverk, H. and Seifert, W., *Behavior of Open Steel Grid Decks Under Static and Fatigue Loads*, Transportation Research Record, (1180), 1988.
[5] Fetzer, P., *Behavior of Open Grid Steel Decks under Service and Fatigue Loads*, Thesis submitted to the Oregon State University, Corvallis, 2013.
[6] ABAQUS /CAE 2019, Dassault systemes, Pawtucket, 2019.

Received: October 27, 2020; Published: November 20, 2020